Observation of Single-Mode, Kelvin-Helmholtz Instability in a Supersonic Flow

W. C. Wan,[1,*] G. Malamud,[1,2,†] A. Shimony,[2,3] C. A. Di Stefano,[1] M. R. Trantham,[1] S. R. Klein,[1] D. Shvarts,[1,2,3] C. C. Kuranz,[1] and R. P. Drake[1]

[1]*Climate and Space Sciences and Engineering, University of Michigan, Ann Arbor, MI 48109, USA*
[2]*Nuclear Research Center – Negev, Beer Sheva 84190, Israel*
[3]*Department of Physics, Ben Gurion University of the Negev, Beer Sheva 84190, Israel*

(Received 3 December 2014; revised manuscript received 12 June 2015; published 1 October 2015)

We report the first observation, in a supersonic flow, of the evolution of the Kelvin-Helmholtz instability from a single-mode initial condition. To obtain these data, we used a novel experimental system to produce a steady shock wave of unprecedented duration in a laser-driven experiment. The shocked, flowing material creates a shear layer between two plasmas at high energy density. We measured the resulting interface structure using radiography. Hydrodynamic simulations reproduce the large-scale structures very well and the medium-scale structures fairly well, and imply that we observed the expected reduction in growth rate for supersonic shear flow.

DOI: 10.1103/PhysRevLett.115.145001 PACS numbers: 52.35.Tc, 47.20.Ft, 47.40.Ki, 52.38.-r

The Kelvin-Helmholtz (KH) instability [1,2], which can produce vortical structures and turbulence, is ubiquitous in shear flows, and is responsible for intermixing of materials in both natural and engineering systems. The flows in stellar processes [3,4], astrophysical jets [5], and protoplanetary disks [6] are typically supersonic. Compressibility becomes significant in supersonic flows, altering the evolution of the instability so that the KH behavior in such flows is an important topic of fundamental interest. Here we report the first experimental observation of structure produced by KH evolving from a well-controlled, single-mode initial condition in a steady, supersonic, compressible flow.

The growth and saturation of single KH modes, producing features described as "rollups," is a fundamental building block of all more-complex KH evolution. Past work has been unable to observe single-mode KH behavior in the supersonic regime. Work producing supersonic merged flows over wedges [7] or counterstreaming supersonic flows with no seed modulation [8] generated uncontrolled, multimode initial conditions that precluded single-mode observations. Other recent work observed the growth of (random) multimode KH driven by subsonic, shear flow [9,10]. The single-mode experiment of Harding *et al.* [11] produced rollups via a different mechanism: the baroclinic ($\nabla\rho \times \nabla p$) deposition of vorticity by laser-driven shock fronts, with negligible contributions from the later, subsonic shear flow. (Here p is pressure and ρ is density.)

The present experiment also establishes a platform that can be iterated to explore compressible, high-energy-density, shear flows in more detail. Without experiments, we do not know to what extent the development of structure or turbulence at small scales will affect the evolution of large-scale structures [12], but we do know [13,14] that such effects exist in incompressible flows. The evolution of shear flows in dense, compressible plasmas might also be altered by heat conduction, actual material structure, or the many small shock waves present. Among several other possible factors, uncertainties associated with these issues might contribute to the inability to predict recent experiments at the National Ignition Facility [15,16]. The relevant codes have only been validated against the large-scale structures of shear flow. The present experiment, and future experiments using this platform, can provide a higher level of validation of predictions of small-scale turbulent structures [17].

We designed our experiment so that the growth would be primarily due to shear flow and so that compressible (i.e., supersonic) effects would be significant. The choice of conditions was based on the exponential growth rate for small-amplitude modes, which characterizes the strength of the instability, even in the nonlinear regime. For the relevant conditions in which there is no surface tension, and gravitational acceleration and viscous effects are negligible, and in which a thin velocity shear layer is located at an interface between two fluids, the growth rate for subsonic, incompressible flows [18] is

$$\gamma_{\mathrm{ic}} = \frac{k\Delta u}{2}\frac{\sqrt{\rho_1\rho_2}}{\rho_1+\rho_2} = \frac{k\Delta u}{2}\sqrt{1-A^2}. \tag{1}$$

The wave number of the modulation is k, the difference in velocity across the interface is Δu, the subscript on the density designates a specific fluid region, and the Atwood number A is $(\rho_2-\rho_1)/(\rho_2+\rho_1)$. The growth rate for compressible flows [19,20] is

$$\gamma = \gamma_{\mathrm{ic}}\frac{\sqrt{-1-M_c^2+\sqrt{1+4M_c^2}}}{M_c}, \tag{2}$$

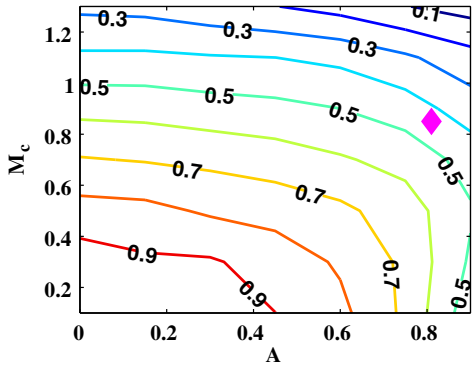

FIG. 1 (color online). The ratio of compressible to incompressible growth rate coefficients, γ/γ_{ic}, in the $M_c - A$ plane. The diamond at $M_c = 0.85$, $A = 0.81$ represents our experiment. Note that, because of the definition of M_c, the supersonic regime corresponds to $M_c > 0.5$.

where the convective Mach number, M_c, is defined as $\Delta u/(c_1 + c_2)$, with c being the speed of sound. (In the frame of reference of either fluid, the condition on M_c for the flow to be supersonic in the usual sense is that $M_c \gtrsim 0.5$). Figure 1 shows the ratio γ/γ_{ic} as a function of A and M_c [21]. For the parameters of the experiment, compressible effects are predicted to reduce the small-amplitude growth rate by a factor of 2.

The experimental design [21] exploited the long pulses available on Omega EP [22] to create sustained, steady, laser-driven shocks of unprecedented duration. We drove the experiment using three sequential laser beams, each having a ~10-ns pulse and wavelength of 351 nm. This produced a 28-ns, 12.5-kJ nominally square pulse with a 300-ps rise time, striking a 1.1-mm diameter spot (created by distributed phase plates) to produce an irradiance of $\sim 4.2 \times 10^{13}$ W/cm^2. The resulting ablation pressure and shocked material sustained the shock wave until ~70 ns, where $t = 0$ corresponds to the time of initiation of the first laser pulse. Figure 2 shows the laser target and the properties of each layer. The steady shock wave propagated through the ablator and then through a thermal insulator of nearly the same density, present to prevent preheating of the structured interface.

At the rear of the insulator, and in the top half of the target, this shock then reached a layer of low-density foam. In response, a shock wave propagated through the foam, while a rarefaction returned through the insulator and ablator. The thickness of the ablator was chosen so that the eventual return wave from the ablation surface would not reach the evolving modulations on experimental time scales, throughout which the shock wave in the foam was sustained and steady. In the lower half of the target, the incoming shock wave was retarded by a layer of dense tin. The shock wave in the foam moved quickly across the tin and then generated shear across a plastic surface onto which the a modulation had been machined, having a 100-μm wavelength, λ, and a 5-μm amplitude. The ~0.63-Mbar pressure in the shocked foam drove a shock wave into this plastic material, converting it to plasma and deflecting the foam-plastic interface. We refer to the angle between the unshocked interface and the deflected interface as the deflection angle.

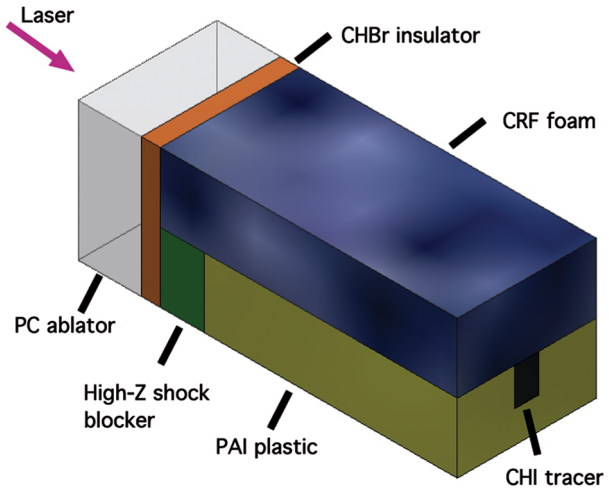

FIG. 2 (color online). Schematic view of the target. The ablator is a 500-μm-thick layer of polycarbonate (PC) ($C_{16}H_{14}O_3$, $\rho = 1.08$ g/cm^3). The insulator is a 150-μm-thick layer of brominated plastic (CHBr) ($C_{50}H_{48}Br_2$, $\rho = 1.17$ g/cm^3). The low-density layer is carbonized-resorcinol-formaldehyde foam (CRF) ($C_{1000}O_{48}H_{65}$, $\rho = 0.10$ g/cm^3). The high-Z shock blocker is a 350-μm-thick layer of Sn (7.3 g/cm^3). The plastic block consists of a high-density polyamide-imide (PAI) ($C_{22}H_{14}O_4N_2$, $\rho = 1.40$ g/cm^3), containing a 190-μm-wide iodinated polystyrene (CHI) ($C_{50}H_{47}I_3$, $\rho = 1.44$ g/cm^3) tracer strip of nominally equal density.

Figure 3 shows the anticipated experimental system after the shock wave has propagated about 1 mm through the foam. The design simulations [21] used the DAFNA code in 2D, initialized with a shock-Hugoniot condition based on 1D radiation hydrodynamic modeling using HYADES [23]

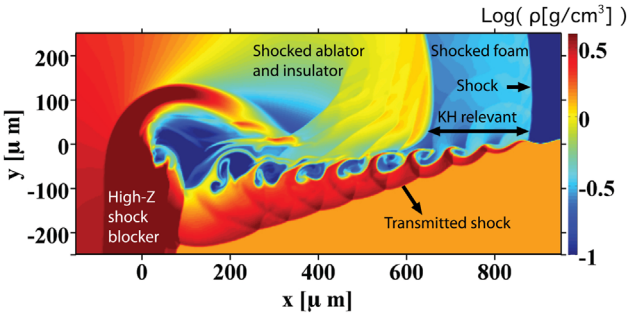

FIG. 3 (color online). 2D DAFNA simulation showing log (density[g/cm^3]) at $t = 65$ ns. The sustained drive pressure produces a steady postshock velocity in the foam to drive KH growth. The part of the system relevant here is the shocked foam, where the ablator and insulator material do not interfere with the dynamics.

and treating the foam as an ideal gas with an adjustable adiabatic index. DAFNA is a multimaterial Harten-Lax-van Leer-Contact-based Eulerian code with interface tracking and adaptive mesh refinement capabilities. HYADES is a Lagrangian radiation-hydrodynamic code including a laser-absorption model. Additional 2D modeling with CRASH [24], which has a multidimensional laser package, also confirms the modeling of the laser-driven behavior. The experiment was designed so that the vorticity produced by baroclinic effects was small compared to that driven by the steady, shear flow. Unfortunately, this experimental approach does not enable one to vary M_c significantly.

We measured the interface structure radiographically. The measurement used a spherical crystal imager [25] to image Cu K_α x rays, produced by irradiating a 1-mm-diameter Cu foil with 850 J of laser light of 1053-nm wavelength, focused to a 200-μm-diameter spot, in a 10-ps pulse, at a selected time of interest. These x rays propagated through the target and to the crystal, which imaged them onto a Fuji™ MS image plate [26]. The modulated plastic layer included the tracer strip shown in Fig. 2, which localized the x ray opacity in the central portion of the target so that the structure seen in the image is not complicated by effects from the edges of the target along the line of sight. We obtained images from 40 to 65 ns. Figure 4(a) shows an example of the resulting data, in which the growing modulations can be clearly seen.

We processed the radiographic data using an unsharp-mask algorithm [10,21] to obtain the interface location, and analyzed the results to infer several quantities of interest, shown in Table I. We determined the shock location for each radiograph by locating the position where the surface of the plastic was deflected downward, and inferred the shock velocity from these observations at various times. We obtained the compression by fitting the motion of the shock wave and the thermal insulator, and inferred the shear velocity using the basic shock equations. Note also that shock compression causes the spacing of the rollups to be smaller than the initial imposed wavelength [21]. In the table, we also show the same quantities from the simulation of Fig. 3. The simulation used the actual experimental dimensions and was the result of fine-tuning the Mach number and the adiabatic index of the foam, in order to match the observed shock timing and interface deflection. We can see that other parameters found by the simulation match those inferred from the data to within the experimental uncertainties.

These parameters can be used to estimate the rate at which the system could transition to turbulence. The modulations curl into vortical structures with a characteristic large-eddy timescale for turbulent evolution given as $\tau = \lambda/\Delta u$ [27]. Classically, this value is used to approximate the time it takes for a modulation to curl around itself once in an incompressible shear flow with homogeneous turbulence. The parameters listed in Table I imply that the oldest undisturbed modulations have been allowed to evolve for 2τ–3τ, long enough to have plausibly developed a turbulent interior, despite effects of compressibility and inhomogeneity [21]. Here, we define medium-scale structures to be on the order of 10 to 15 μm, which is at the edge of our diagnostic resolution [25]. An example of medium-scale structure is the curled tip that arises as a modulation evolves, whereas the peak-to-valley amplitude of the vortices is an example of large-scale structure.

Figure 4(c) compares the results of DAFNA simulations with the data by overplotting the interface location found from a simulated radiograph (including realistic noise) upon the contrast-enhanced data of Fig. 4(b). One would expect the simulations to become less accurate at progressively smaller relative scales. One can see that the code

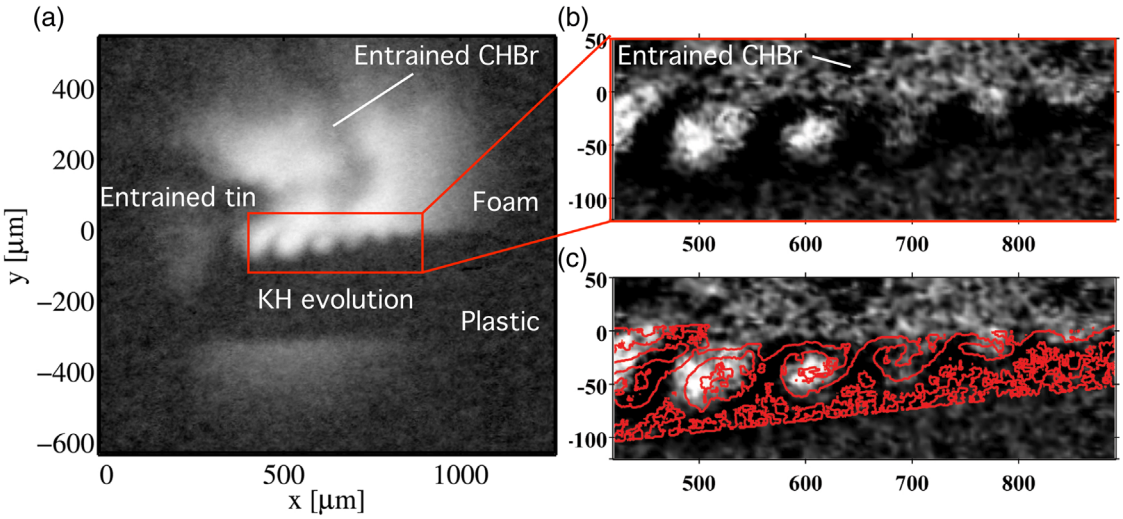

FIG. 4 (color online). (a) Raw radiographic image at t = 65 ns. (b) Contrast-enhanced data. (c) Interface extracted from the DAFNA simulated radiograph (red lines) overlaid on the processed experimental data.

TABLE I. Experimentally inferred parameters are compared to their predicted values.

Parameter	Experiment	Simulation
Shock velocity u_s (μm/ns)	28 ± 2	29
Deflection angle (°)	7.7 ± 1.2	8.3
Foam compression	5.0 ± 1.5	4
Shocked foam pressure (Mbar)	0.63 ± 0.08	0.59
Shear velocity Δu (μm/ns)	22 ± 3	20
Rollup spacing λ (μm)	77 ± 6	80

reproduces the large-scale structures very well, as one would expect. It reproduces the medium-scale structures fairly well, and one cannot readily determine whether the apparent differences reflect a real difference or just experimental uncertainty. One can also infer that differences in small-scale structure between the simulation and the experiment did not in this case affect the large-scale structures significantly. Improvements to the experiment, using the platform demonstrated here, could proceed to explore such scales including the mixing of material into the interior of the rollups.

In order to assess the importance of compressible effects on large-scale behavior, we also performed simulations of pure shear flow. The simulations used the experimental densities and shear velocities. One of them simulated a compressible case, using a pressure (and, hence, sound speed) taken from the DAFNA simulations so that $M_c = 0.85$ as in the experiment. The other simulated a nearly incompressible case, by using a higher pressure (and, hence, sound speed), so that $M_c = 0.1$. To interpret the results, it is helpful to recall that single vortices eventually reach a (full) saturated amplitude of 0.56 times their spacing, after which their amplitudes oscillate [28–30]. As a result, the impact of a smaller growth rate is to delay the growth but not ultimately to change the saturated amplitude. Figure 5 shows a comparison of the data and the simulations using pure shear flow. The abscissa is the dimensionless evolution time appropriate to shear-driven flow, $\Delta u t_s/\lambda$, where t_s is the time since the passage of the shock, i.e., the time for which the KH has been developing. In addition, the period before which the passage of the insulator material alters the dynamics extends to $\Delta u t_s/\lambda \sim 4$, so that data beyond this value may exhibit altered behavior.

Comparisons of the data and the simulations using pure shear flow support the conclusion that compressibility affects KH evolution. Figure 5 plots the modulation amplitude from the two simulations against the measured experimental amplitude. To do so, we found the experimental amplitude by rotating the image so that an interface deflected by 7.7° (the measured average) would be horizontal, using the shock front to define $t_s = 0$. The height is calculated as the difference between how far a given central

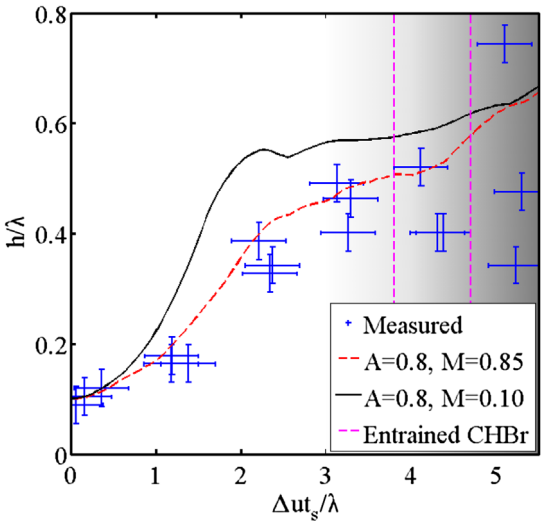

FIG. 5 (color online). Normalized experimental data fit against theoretical predictions with (dashed red) and without (solid black) significant compression. The dashed magenta lines at $\Delta u t_s/\lambda \sim 4$ represent the location of the CHBr insulator layer, which disturbs the evolving modulations.

peak of the heavy fluid has penetrated into the lighter fluid, and the average of how far the lighter fluid has penetrated into the heavy fluid on either side of the central peak. The vertical error bars are determined from the resolution limit of the diagnostic. We found the corresponding amplitude from the simulations, with respect to the location of the interface in a simulation without a seed perturbation [21]. One sees that the dashed curve, from the simulation having $M_c = 0.85$, matches the growth of the modulations, while the curve from the $M_c = 0.10$ simulation does not. We can see that across all the data, until $\Delta u t_s/\lambda \sim 4$, the amplitude from the simulation of the compressible case is reasonably consistent with the data and that, in contrast, the amplitude from the simulation of the incompressible case is not, over most of the relevant period.

In summary, we have reported the first observations of the evolution of single-mode modulations under the influence of the Kelvin-Helmholtz instability in a supersonic flow. We obtained these data by using a novel experimental system to produce a steady shock wave of unprecedented duration, and using the shocked, flowing material to create a shear layer between two plasmas at high energy density. Our data can be used to benchmark hydrodynamic models or nonlinear theories. Future work can explore multimode behavior and, ultimately, the transition to turbulence.

The authors acknowledge the OMEGA-EP Operations Staff, General Atomics, and Michigan Target Fabrication for their outstanding support. This work is funded by the U.S. Department of Energy, through the NNSA-DS and SC-OFES Joint Program in High-Energy-Density Laboratory Plasmas, Grant No. DE-NA0001840, and the

National Laser User Facility Program, Grant No. DE-NA0002032, and through the Laboratory for Laser Energetics, University of Rochester by the NNSA/OICF under Cooperative Agreement No. DE-FC52-08NA28302.

*Corresponding author.
wwan@umich.edu
†Corresponding author.
guy.malamud@gmail.com

[1] W. Thomson (Lord Kelvin), Hydrokinetic solutions and observations, Philos. Mag. (1798–1977) **42**, 362 (1871).
[2] H. Helmholtz, Über discontinuierliche flüssigkeits-bewegungen (on the discontinuous movements of fluids), Philos. Mag. (1798–1977) **36**, 337 (1868).
[3] L. Feng, B. Inhester, and W. Q. Gan, Kelvin-Helmholtz instability of a coronal streamer, Astrophys. J. Lett. **774**, 141 (2013).
[4] J. Guzman and T. Plewa, Nonspherical core-collapse supernovae: Evolution towards homologous expansion, Nonlinearity **22**, 2775 (2009).
[5] C. L. Gardner and S. J. Dwyer, Numerical simulation of the {XZ} tauri supersonic astrophysical jet, Acta Mathematica Scientia **29**, 1677 (2009).
[6] P. Garaud and D. N. C. Lin, On the evolution and stability of a protoplanetary disk dust layer, Astrophys. J. **608**, 1050 (2004).
[7] M. D. Slessor, M. Zhuang, and P. E. Dimotakis, Turbulent shear-layer mixing: Growth-rate compressibility scaling, J. Fluid Mech. **414**, 35 (2000).
[8] F. W. Doss, E. N. Loomis, L. Welser-Sherrill, J. R. Fincke, K. A. Flippo, and P. A. Keiter, Instability, mixing, and transition to turbulence in a laser-driven counterflowing shear experiment, Phys. Plasmas **20**, 012707 (2013).
[9] V. A. Smalyuk, J. F. Hansen, O. A. Hurricane, G. Langstaff, D. Martinez, H.-S. Park, K. Raman, B. A. Remington, H. F. Robey, O. Schilling, R. Wallace, Y. Elbaz, A. Shimony, D. Shvarts, C. Di Stefano, R. P. Drake, D. Marion, C. M. Krauland, and C. C. Kuranz, Experimental observations of turbulent mixing due to Kelvin-Helmholtz instability on the Omega laser facility, Phys. Plasmas **19**, 092702 (2012).
[10] C. A. Di Stefano, G. Malamud, M. T. Henry de Frahan, C. C. Kuranz, A. Shimony, S. R. Klein, R. P. Drake, E. Johnsen, D. Shvarts, V. A. Smalyuk, and D. Martinez, Observation and modeling of mixing-layer development in high-energy-density, blast-wave-driven shear flow, Phys. Plasmas **21**, 056306 (2014).
[11] E. C. Harding, J. F. Hansen, O. A. Hurricane, R. P. Drake, H. F. Robey, C. C. Kuranz, B. A. Remington, M. J. Bono, M. J. Grosskopf, and R. S. Gillespie, Observation of a Kelvin-Helmholtz Instability in a High-Energy-Density Plasma on the Omega Laser, Phys. Rev. Lett. **103**, 045005 (2009).
[12] V. A. Smalyuk, R. E. Tipton, J. E. Pino, D. T. Casey, G. P. Grim, B. A. Remington, D. P. Rowley, S. V. Weber, M. Barrios, L. R. Benedetti, D. L. Bleuel, D. K. Bradley, J. A. Caggiano, D. A. Callahan, C. J. Cerjan, D. S. Clark, D. H. Edgell, M. J. Edwards, J. A. Frenje, M. Gatu-Johnson *et al.*, Measurements of an Ablator-Gas Atomic Mix in Indirectly Driven Implosions at the National Ignition Facility, Phys. Rev. Lett. **112**, 025002 (2014).
[13] B. D. Collins and J. W. Jacobs, Plif flow visualization and measurements of the Richtmyer-Meshkov instability of an air/sf6 interface, J. Fluid Mech. **464**, 113 (2002).
[14] J. T. Waddell, C. E. Niederhaus, and J. W. Jacobs, Experimental study of Rayleigh-Taylor instability: Low Atwood number liquid systems with single-mode initial perturbations, Phys. Fluids **13**, 1263 (2001).
[15] A. B. Zylstra, J. A. Frenje, F. H. Sguin, D. G. Hicks, E. L. Dewald, H. F. Robey, J. R. Rygg, N. B. Meezan, M. J. Rosenberg, H. G. Rinderknecht, S. Friedrich, R. Bionta, R. Olson, J. Atherton, M. Barrios, P. Bell, R. Benedetti, L. Berzak Hopkins, R. Betti, D. Bradley *et al.*, The effect of shock dynamics on compressibility of ignition-scale national ignition facility implosions, Phys. Plasmas **21**, 112701 (2014).
[16] J. D. Moody, D. A. Callahan, D. E. Hinkel, P. A. Amendt, K. L. Baker, D. Bradley, P. M. Celliers, E. L. Dewald, L. Divol, T. Döppner, D. C. Eder, M. J. Edwards, O. Jones, S. W. Haan, D. Ho, L. B. Hopkins, N. Izumi, D. Kalantar, R. L. Kauffman, J. D. Kilkenny *et al.*, Progress in hohlraum physics for the National Ignition Facility, Phys. Plasmas **21**, 056317 (2014).
[17] M. M. Marinak, G. D. Kerbel, N. A. Gentile, O. Jones, D. Munro, S. Pollaine, T. R. Dittrich, and S. W. Haan, Three-dimensional HYDRA simulations of National Ignition Facility targets, Phys. Plasmas **8**, 2275 (2001).
[18] S. Chandrasekhar, Hydrodynamic and hydromagnetic stability, in *International Series of Monographs on Physics* (Clarendon Press, Oxford, 1961).
[19] L. D. Landau, Stability of a tangential discontinuity in a compressible liquid, Dokl. Akad. Nauk SSSR **44**, 151 (1944).
[20] S. Roy Choudhury, Nonlinear evolution of the Kelvin-Helmholtz instability of supersonic tangential velocity discontinuities, J. Math. Anal. Appl. **214**, 561 (1997).
[21] G. Malamud, A. Shimony, W. C. Wan, C. A. Di Stefano, Y. Elbaz, C. C. Kuranz, P. A. Keiter, R. P. Drake, and D. Shvarts, A design of a two-dimensional, supersonic KH experiment on Omega EP, High Energy Density Phys. **9**, 672 (2013).
[22] D. N. Maywar, J. H. Kelly, L. J. Waxer, S. F. B. Morse, I. A. Begishev, J. Bromage, C. Dorrer, J. L. Edwards, L. Folnsbee, M. J. Guardalben, S. D. Jacobs, R. Jungquist, T. J. Kessler, R. W. Kidder, B. E. Kruschwitz, S. J. Loucks, J. R. Marciante, R. L. McCrory, D. D. Meyerhofer, A. V. Okishev *et al.*, Omega EP high-energy petawatt laser: Progress and prospects, J. Phys. Conf. Ser. **112**, 032007 (2008).
[23] J. T. Larsen and S. M. Lane, Hyades—plasma hydrodynamics code for dense plasma studies, J. Quant. Spectrosc. Radiat. Transfer **51**, 179 (1994).
[24] B. van der Holst, G. Tóth, I. V. Sokolov, K. G. Powell, J. P. Holloway, E. S. Myra, Q. Stout, M. L. Adams, J. E. Morel, S. Karni, B. Fryxell, and R. P. Drake, Crash: A block-adaptive-mesh code for radiative shock hydrodynamics implementation and verification, Astrophys. J. Suppl. Ser. **194**, 23 (2011).

[25] C. Stoeckl, G. Fiksel, D. Guy, C. Mileham, P. M. Nilson, T. C. Sangster, M. J. Shoup, and W. Theobald, A spherical crystal imager for Omega EP, Rev. Sci. Instrum. **83**, 033107 (2012).

[26] B. R. Maddox, H. S. Park, B. A. Remington, N. Izumi, S. Chen, C. Chen, G. Kimminau, Z. Ali, M. J. Haugh, and Q. Ma, High-energy x-ray backlighter spectrum measurements using calibrated image plates, Rev. Sci. Instrum. **82**, 023111 (2011).

[27] U. Frisch, Phenomenology of turbulence in the sense of Kolmogorov 1941, in *Turbulence: The Legacy of A.N. Kolmogorov* (Cambridge University Press, Cambridge, England, 1995).

[28] A. Rikanati, U. Alon, and D. Shvarts, Vortex-merger statistical-mechanics model for the late time self-similar evolution of the Kelvin-Helmholtz instability, Phys. Fluids **15**, 3776 (2003).

[29] P. C. Patnaik, F. S. Sherman, and G. M. Corcos, A numerical simulation of Kelvin-Helmholtz waves of finite amplitude, J. Fluid Mech. **73**, 215 (1976).

[30] C. Pozrikidis and J. J. L. Higdon, Nonlinear Kelvin-Helmholtz instability of a finite vortex layer, J. Fluid Mech. **157**, 225 (1985).